

SCIENTIFIC REPORTS



OPEN

Silver oxide decomposition mediated direct bonding of silicon-based materials

Tomoki Matsuda, Kota Inami, Keita Motoyama, Tomokazu Sano  & Akio Hirose

Silicon-based materials are widely promising electronic components by the combination with metals in power electronics field. However, bonding metal and silicon-based materials generally requires specific surface modification due to their different chemical bonds. Here, we demonstrate a process for directly bonding metals to silicon-based materials that does not require surface treatment, based on the *in situ* decomposition of Ag_2O paste, forming Ag nanoparticles (AgNPs). We demonstrate sound joints of Ag/silicon-based materials at 300–500 °C with the formation of a silicon oxide interlayer containing AgNPs. We propose that Ag in the interlayer attracted other Ag particles to the interface, playing a unique role in this direct bonding process. This process is suitable for various bonding applications in electronics, as well the fabrication of conducting paths for photovoltaic and other applications.

The bonding between metal and silicon-based materials (Si-material), such as silicon carbide (SiC), a wide-bandgap semiconductor, and silicon dioxide (SiO_2), used as gate oxide in metal-oxide-semiconductor (MOS) structures, has attracted growing interest in the recent development of the power electronics field¹. Since covalent and ionic bonds are generally the principal types of chemical bonds in these semiconductors, compatibility with the metallic bonds is greatly limited. Hence, some surface pre-treatments, e.g. metallization, are necessary to facilitate bonding between metal and semiconductors (or various ceramics)^{2–5}. For example, titanium or nickel have been deposited on $\text{Si}^{2,3}$ and $\text{SiC}^{4,5}$ substrates. Hence, conventional metal-to-ceramic bonding involves indirect processes.

A bonding method involving the sintering of Ag derived from the redox reaction between Ag_2O and an organic solvent has been reported^{6,7}: Ag nanoparticles (AgNPs) are generated during the bonding process as a result of the redox reaction. Nanoparticles smaller than 10 nm show an apparent melting-point depression^{8–10} caused by the high surface to volume ratio¹¹, making them more reactive. Recent studies reported that, not only metals^{12–14}, but some aluminium oxide ceramics (e.g. Al_2O_3), can be bonded using this method¹⁵. In particular, a typical bonding mechanism of Ag to Al_2O_3 was suggested; Ag ions temporarily generated during the redox reaction attach to the Al_2O_3 surface, leading to the formation of an initial Ag layer that facilitates the sintering of the AgNPs. Thus, an application of the bonding method to ceramics with high ion-binding properties was proposed. However, very little is known about the bonding morphology between the Ag and Si-materials as they have the high covalent properties, which requires surface pre-treatments even when using the AgNP joining process^{4,16}.

Many studies have been conducted on the diffusivity of Ag into SiO_2 and the adhesion between these materials^{17–23}. The adhesion and diffusion of Ag into pure SiO_2 is often difficult¹⁷, unlike some glasses containing sodium or potassium, e.g. soda-lime glass, into which Ag diffuses easily due to the ion exchange reaction^{18,19}. The attraction of Ag ions to the SiO_2 surface is enhanced after surface chemical treatments^{20,21}, such as amination or the rupture of Si–O–Si bonds by ultrasonic radiation²² or electron irradiation²³. It was also shown that the diffusion of metallic ions into SiO_2 is facilitated under an electric field^{24,25}. The diffusion of Ag ions into SiO_2 without such an external driving force has not been studied in detail to our knowledge, but the formation of metallic ions would be likely to contribute to the bonding of SiO_2 with metals.

During the reaction between Ag_2O and an organic solvent, AgNPs can be produced by two different processes; a redox reaction temporarily producing Ag ions, and thermal decomposition during heating^{26–28}, which can induce the formation of Ag ions or atoms as an intermediate state. A silicon oxide (i.e. SiO_x) layer is generally formed on the surface of Si-materials as a native oxide film. We hypothesized that the decomposition of Ag_2O could be used in the bonding of Ag to various Si-materials by taking advantage of the good adhesion between

Division of Materials and Manufacturing Science, Graduate School of Engineering, Osaka University, 2-1 Yamadaoka, Suita, Osaka, 565-0871, Japan. Correspondence and requests for materials should be addressed to T.M. (email: t-matsu@mapse.eng.osaka-u.ac.jp)

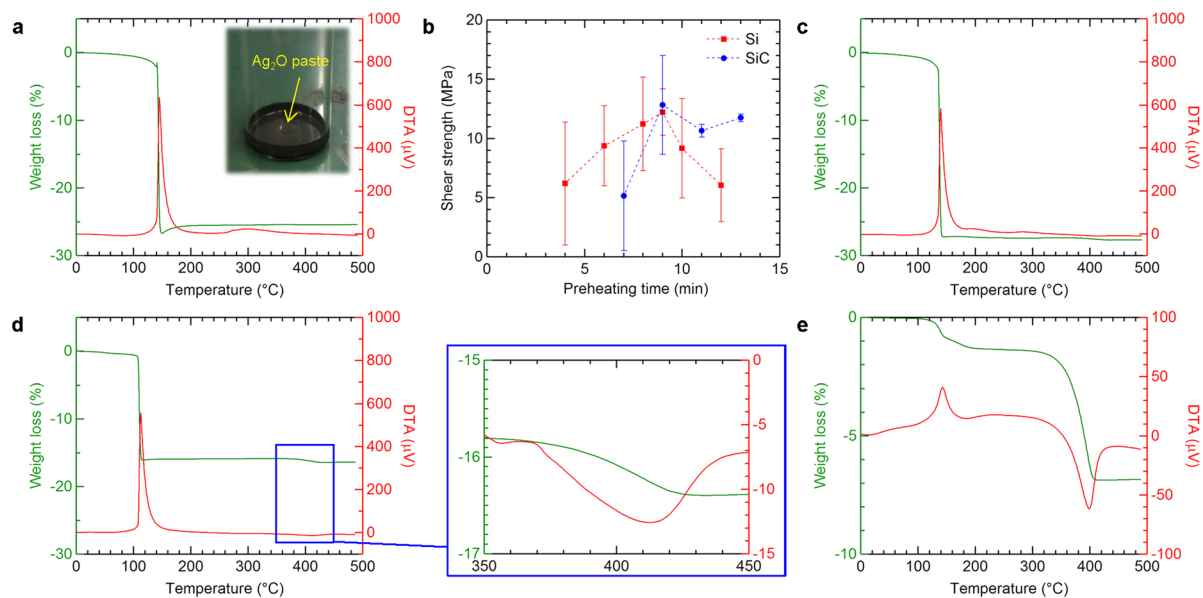


Figure 1. Weight loss and heat of reaction behaviour during heating to the bonding temperature. **(a)** TGA-DTA curves for the paste without preheating; the inset shows a photograph of the Ag_2O paste used in this study. **(b)** Shear strength of the joint bonded at 400°C after preheating at 100°C for various holding times. **(c–e)** TGA-DTA curves for the paste after preheating for **(c)** 3 min, **(d)** 9 min, and **(e)** 13 min, where the positive/negative DTA values refer to exothermic/endothermic reactions, respectively.

the intermediate forms of Ag and the silicon oxide. Here, we report the direct bonding of Si-materials, such as Si, SiO_2 , and SiC, by Ag sintering derived from the two different decomposition reactions of Ag_2O . For the bonding of Si-materials, a thermal process was firstly designed based on the investigation of the decomposition behaviour of a paste comprising Ag_2O and organic solvent using thermal analysis. Then, the influence of the bonding temperature on the joint strength was evaluated in addition to interfacial microstructural observations. Finally, the adhesion behaviour of the AgNP on the SiO_2 substrate was modelled and compared to the experimental results.

Results

Evaluation of the bond quality of silicon-based materials. To utilize the decomposition reaction of a paste comprising Ag_2O and diethylene glycol ($\text{C}_4\text{H}_{10}\text{O}_3$), control of the preheating before the bonding is useful in order to remove excess solvent, which is likely to hinder the sintering of particles. In addition, it is also necessary to limit the preheating temperature below the reduction temperature to avoid promoting this reaction, as the initial formation of excess amounts of AgNPs during the preheating process could result in their cohesion and inhibition of sintering. Figure 1(a) shows thermogravimetric analysis-differential thermal analysis (TGA-DTA) results of the Ag_2O paste with increasing temperature. An exothermal DTA peak accompanied by significant weight loss in TGA was measured at 145°C ; it was reported that the redox reaction of Ag_2O exhibits an exothermic reaction above 100°C ^{13,14}. Subsequently, another exothermic DTA peak was also measured at 297°C , attributed to the decomposition of the organic solvent around 300°C . The optimum preheating temperature was therefore chosen as 100°C . The preheating time appropriate for bonding was investigated based on an evaluation of the bond quality. Figure 1(b) shows the shear strength of joints between Si-materials (Si and SiC) and Au using the Ag layer bonding method at 400°C plotted against preheating time over the range of 2–13 min. The shear strength of both joints increased upon reaching 9 min, above which it decreased again. In order to verify the behaviour before and after 9 min, TGA-DTA curves were measured as a function of temperature for samples preheated for 3, 9, or 13 min, as shown in Fig. 1(c–e), respectively. For the short preheating time of 3 min (Fig. 1(c)), a slight exothermic DTA peak was observed, indicating the presence of remaining solvent. An endothermic DTA peak accompanied by weight loss was observed from 350 to 400°C for the moderate and long preheating times of 9 min and 13 min, respectively (Fig. 1(d,e)). Endothermic reactions generally occur during the thermal decomposition of Ag_2O at around 400°C ^{19,26}. It should be noted that the rate of weight loss during the reduction of Ag_2O decreased with increasing preheating time. The results revealed that the amount of reduced Ag decreased because of excess volatilization of organic solvent during preheating. Hence, it is considered that remaining Ag_2O particles that were not fully reduced by the organic solvent were thermally decomposed in the case of longer preheating times. Further, the slight thermal decomposition behaviour may have contributed to the bonding because the behaviour was also confirmed in appropriate preheating time for joint shear strength (Fig. 1(d)). Thus, the bonding process was performed with a preheating time of 9 min at 100°C .

Figure 2 shows the shear strength of the joint between Au and Si-materials bonded by the sintering of Ag derived from the decomposition of Ag_2O . It was found that the bonding temperature influenced the shear strength of the Si and SiC joints. Both joints showed maximum shear strengths comparable to that of Pb-5Sn solder (18 – 25 MPa)^{29,30}. Hence, we achieved good bonding of Au to Si or SiC without any surface modification.

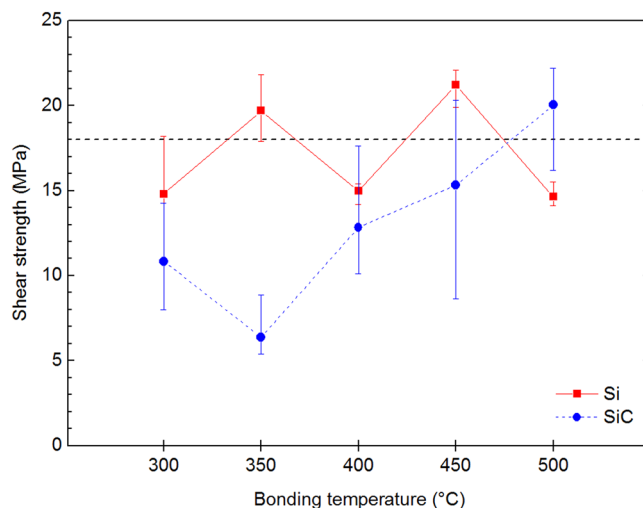


Figure 2. Shear strength of the joints between Si-materials and Au prepared via AgNP sintering. Si-Au and SiC-Au joints prepared at 300–500 °C were tested.

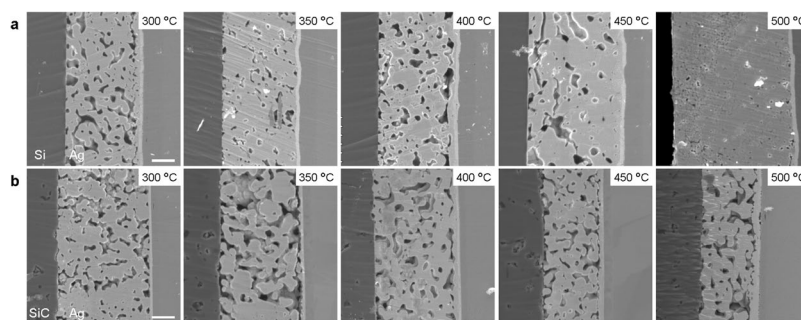


Figure 3. Cross-sectional microstructures of the joints between Si-materials and Au showing the porosity of the Ag layer as a function of temperature. (a) Si-Au and (b) SiC-Au joints at bonding temperature of 300, 350, 400, 450, and 500 °C. Scale bars: 5 μm . All images have the same magnification.

On the other hand, a decrease in the strength occurred for both the Si and SiC joints around 350–400 °C. The fracture in the Si and SiC joints occurred in the sintered Ag layer for almost all bonding temperatures, except for 500 °C, where it occurred in the Si substrate in the Si joint and at the SiC/Ag interface for the SiC joint. Although SiO₂/Ag bonding was also performed at 300–500 °C, the joint shear strength was poor regardless of the bonding temperature. This was because the fracture occurred in the SiO₂ substrate, revealing that the SiO₂/Ag interface was well bonded. The change in the fracture location with increasing bonding temperature indicates increased thermal stresses acting at the interface or substrate. The thermal stress results in the degradation of the joint strength caused by thermal shock, particularly for brittle materials such as Si and SiO₂.

Figure 3 show cross-sectional SEM images of the Si and SiC joints bonded via the sintered Ag layer from 300 to 500 °C. The sintered Ag sufficiently adhered to the substrates with a few pores; Ag adequately bonded to Au, as observed in previous studies^{7,15}. Depending on the bonding temperature, there were differences in the presence of pores in the Ag layer; the porosity tended to decrease with the increasing temperature. A large porosity was observed for samples prepared at 400 °C for the Si joint and 350 °C for the SiC joint, which are temperatures consistent with those where the shear strength decreased. Further, the fracture locations were almost all in the Ag layer, despite the presence of pores at the interface between the Ag and Si-materials. We assume that the porosity in the Ag layer directly influenced the joint shear strength and that the strength of the Si-materials/Ag interface was comparably higher than that of the Ag layer; the correlation between joint strength and porosity will not be satisfied in the case of low interfacial strength. Hence, direct bonding of Ag and Si-materials would be realized via the formation of a sufficiently strong interface for both Si-materials.

Bonding morphology of Ag onto Si-materials. Figure 4 shows TEM images of the microstructure of the interfaces between Si-materials and Ag obtained at 300 and 500 °C. The Si and SiC joints bonded at 300 °C (Fig. 4(a,b), respectively) showed the sintered Ag adhering well to the substrates. An intermediate layer with a thickness below 5 nm was observed at the interface between the Si-materials and sintered Ag (Fig. 4(c,d)). Since a native oxide usually covers Si-materials (e.g., Supplementary Fig. S1 showing the TEM image of the cross-section of the initial Si substrate before bonding), this layer was expected to correspond to the silicon oxide film. The results revealed that bonding of the Si-material and Ag was achieved via this native oxide layer at 300 °C, which

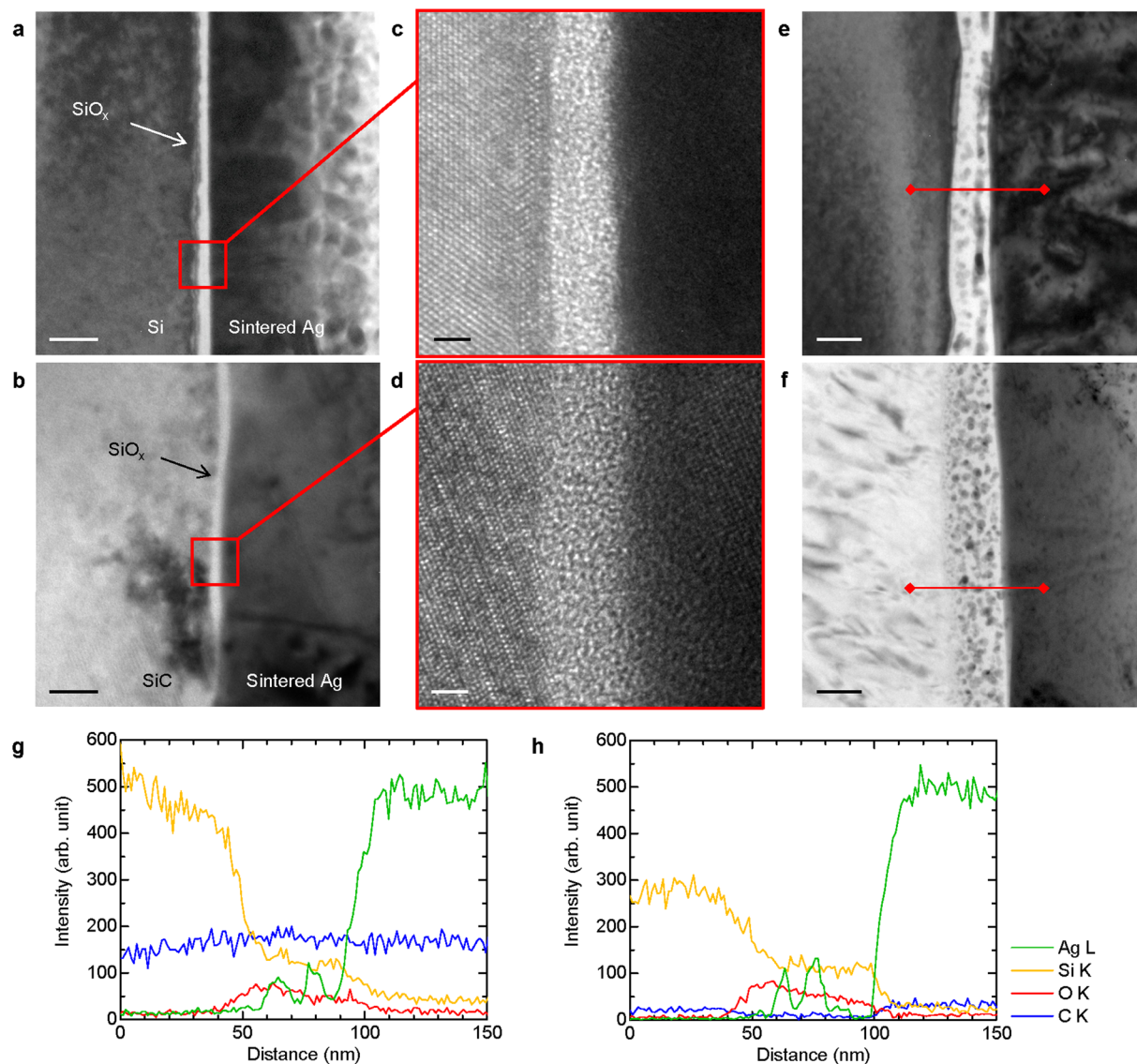


Figure 4. Microstructure and composition of the interface between Si-materials and Ag. Bright-field (BF) TEM image of the interface between (a) Si and Ag and (b) SiC and Ag bonded at 300 °C. (c,d) High-resolution TEM image of (a,b) showing the bonding of Ag and Si-materials via an amorphous native oxide. Interface between (e) Si and Ag and (f) SiC and Ag bonded at 500 °C. (g,h) EDS line analysis for Ag, Si, O, and C along the red line shown in (e,f), respectively. Scale bars, (a,b) 20 nm, (c,d) 2 nm, and (e,f) 50 nm.

is not surprising considering the high quality of the SiO_2 joint. On the other hand, the interfacial microstructure of the Si and SiC joints bonded at 500 °C (Fig. 4(e,f), respectively) were distinctly different from those bonded at 300 °C. The sintered Ag densely bonded to a thicker intermediate layer (50 to 100 nm). In addition, fine particles were present in the intermediate layer for both joints, where the particle size decreased towards the silicon side (from 10 nm at the Ag side to 1 nm at the Si-material side).

EDS line analyses were performed along the red lines shown in Fig. 4(e,f) in order to identify the elemental composition of the intermediate layer and the fine particles. Figure 4(g,h) show the elemental distributions at the interface of Si and SiC joints bonded at 500 °C, respectively, for Si, O, Ag, and C. The O intensity increased at the location of the intermediate layer and Si was also identified. In addition, the intensity of C did not change in the layer. These results reveal that the intermediate layer corresponds to silicon oxide rather than the organic solvent or voids. Both results showed an increase in Ag intensity corresponding to fine particles identified as AgNPs. Therefore, it was found that interfacial bonding between Ag and Si-materials at 500 °C was achieved via a silicon oxide layer containing AgNPs with sizes from several to 10 nm, which were thought to form between 300 °C and 500 °C.

The evolution of the interfacial structure was also observed as a visible colour change in the samples. Figure 5 shows stereomicroscopic images of SiO_2 -Au joints observed from the SiO_2 side (Fig. 5(a)). Although there were no significant differences observed between the joints bonded up to 350 °C, a visible colour change occurred

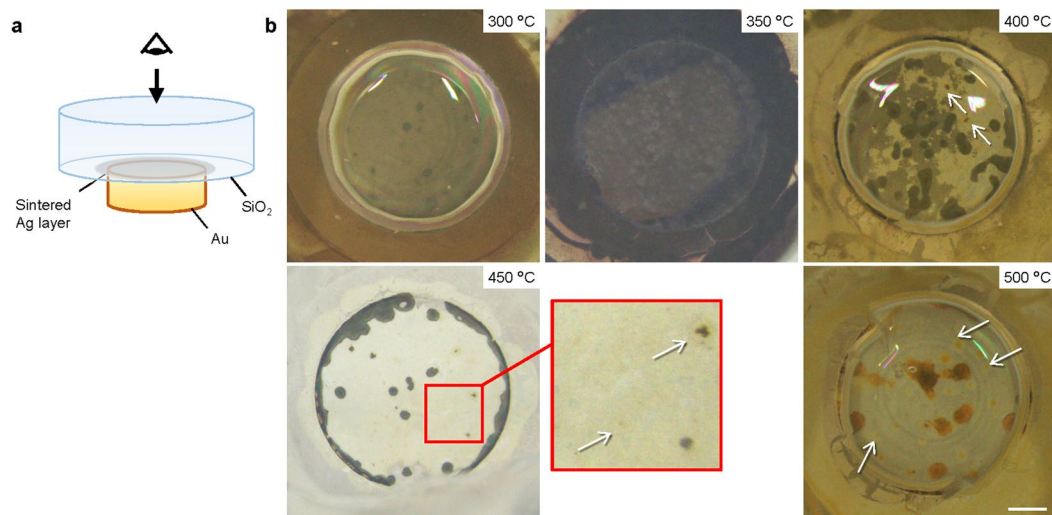
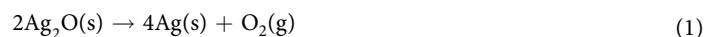


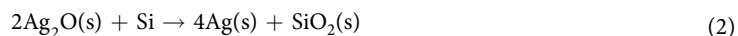
Figure 5. Stereoscopic images showing the visible colour change of SiO₂ bonded to Au using Ag₂O paste as a function of temperature. **(a)** Schematic diagram of the procedure for stereoscopic observation, where the diameter of the Au disc was 5 mm. **(b)** Top views of the interface at 300–500 °C for every 50 °C, where the arrows indicate areas of colour change. The white regions correspond to the sintered Ag layer. Scale bar: 1 mm.

above 400 °C. A few yellow-coloured regions were observed at 400 °C, which increased in size with increasing temperature. Almost the entire bonded region exhibited either a yellow or brown colour at 500 °C. Such visible changes in SiO₂ or silicate glass have been reported as the result of doping with Ag ions, clusters, or NPs (e.g. the use of ion exchange), which implied that the particle growth determined the visible colour change of the glass^{19,31,32}. Particularly, Simo *et al.* reported that Ag ions embedded in a soda-lime silicate glass grew into Ag molecular clusters or NPs at a threshold temperature of 410 °C, accompanied by an obvious colour change¹⁹. Specifically, it was revealed that the change in visible colour corresponded to the growth of AgNPs contained in the SiO₂ layer, where an increase in the thickness of the layer resulted in further colour changes.

The oxidation of Si or SiC does not occur significantly under atmospheric conditions below 500 °C. In contrast, thermal decomposition of Ag₂O occurs around 400 °C (as shown in Fig. 1), which is evident as the colour begins to change. In general, Ag and oxygen were generated during the thermal decomposition of Ag₂O as follows³³:



However, the reaction should actually involve the temporal formation of O before the formation of O₂, resulting in an increase in the oxygen activity. The value of the standard Gibbs free energy change for oxide formation for Si is more negative than that for Ag. Hence, Si can react with oxygen before the formation of gaseous oxygen as follows:



Indeed, Fields reported that the reaction occurred in glass frit bonding³⁴. When Si-materials are oxidized, the volume change ascribed to the reaction generally occurs following the Pilling-Bedworth ratio R_{PB} defined as:

$$R_{PB} = V_{\text{oxide}}/V_{\text{metal}} = M_{\text{oxide}} \cdot \rho_{\text{metal}}/n \cdot M_{\text{metal}} \cdot \rho_{\text{oxide}} \quad (3)$$

where V_m and V_o are the volume of, ρ_m and ρ_o are the densities of the metal and oxide, respectively, M_o and M_m are the atomic mass numbers of the metal and oxide, respectively, and n is the number of metal atoms in the oxide molecule³⁵. R_{PB} for Si/SiO₂ is about 2, while that for SiC/SiO₂ is nearly 1³⁶, generally resulting in differences in the oxide layer roughness. In the present study, the oxide layer produced at the Ag/Si interface was rougher than that for the Ag/SiC sample, which indicates the remarkable oxidation of Si-materials during the thermal decomposition of Ag₂O. It is considered that the formation of a silicon oxide layer containing AgNPs, as shown in Fig. 4(c,d), was induced through thermal decomposition of Ag₂O. Conversely, the joints bonded at low temperature (Fig. 4(a,b)) did not undergo thermal decomposition, implying that Ag was predominantly formed by the redox reaction. Thus, the developed interfacial structure should change according to the thermal decomposition temperature. We note here that almost none of the fracture locations are in the Ag/silicon oxide interface. This suggests that the interfacial strength of Ag/silicon oxide exceeded that of the sintered Ag layer, and also that a strong interfacial bond was already established at 300 °C. Therefore, there is a possibility that the predominant mechanism resulting in the good interfacial strength is similar for both samples before and after thermal decomposition.

Figure 6 shows TEM images of another region of the Ag/Si interface bonded at 300 °C, where the sintered Ag did not bond well to the Si (Fig. 6(a)). Fine particles were present in the white region between the sintered Ag and Si, which adhered well to the thin smooth layer (Fig. 6(b)). Figure 6(c) shows the corresponding EDS maps

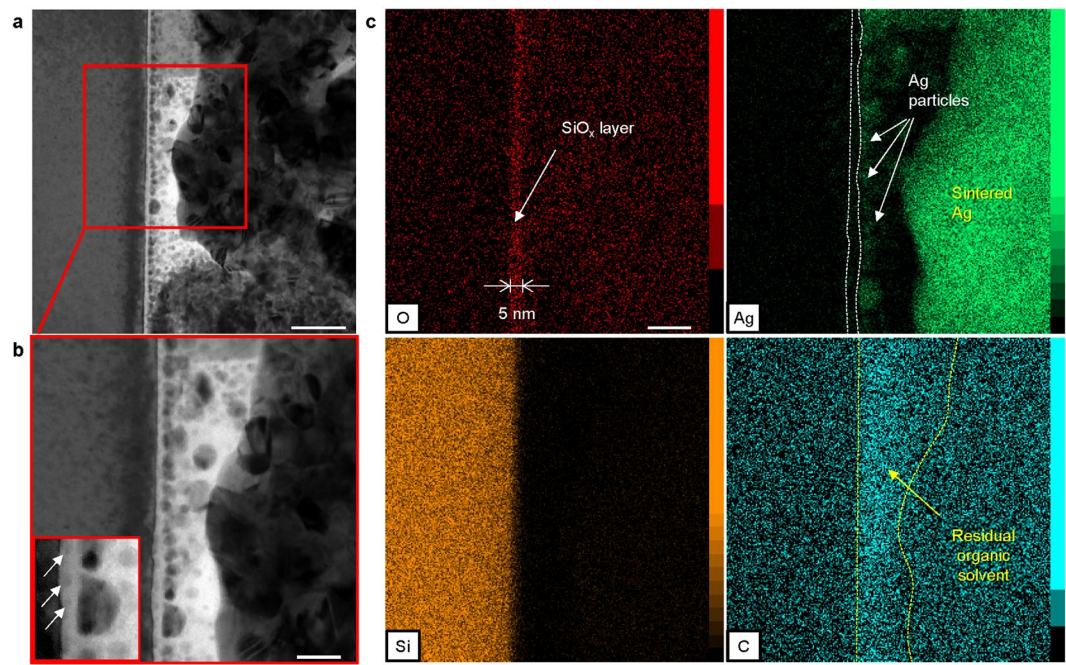


Figure 6. Adhesion of reduced AgNPs onto the native silicon oxide at the Si/Ag interface. **(a)** Bright-field TEM (BF-TEM) image showing the presence of nanoparticles in the thin layer. **(b)** Magnified BF-TEM image of **(a)** showing smaller nanoparticles present within the native oxide. **(c)** EDS mapping of Ag, Si, O, and C. Residual organic solvent hindered the adhesion of the sintered Ag to the silicon oxide. Scale bars: **(a)** 50 nm and **(b,c)** 20 nm.

for O, Ag, Si, and C. It was found that fine particles near the layer were Ag. Unlike the joint bonded at 500 °C, the thickness of the high-O-concentration region was limited to 5 nm, nearly identical to that of the native silicon oxide observed in Fig. 4(a), whereas the concentration of C increased between the silicon oxide and sintered Ag layers. Hence, the white region was identified as residual organic solvent. Residual solvent usually hinders sintering of particles³⁷; hence, this was identified as the reason for the poorly bonded interface. On the other hand, we assumed that the interfacial structure with insufficient sintering was equivalent to that developed from the intermediate state during bonding. These results imply that AgNPs could sufficiently adhere to the silicon oxide layer. It was also confirmed that some particles (~several nm) were present near the Si substrate inside the native oxide, as shown in Fig. 6(a), and that the sintered Ag layer penetrated the native oxide layer, as shown in the inset of Fig. 4(a).

Discussion

Here we discuss the bonding process at each temperature range. Various processes are typically used to achieve AgNPs inside silicon oxide, e.g. using ion-implantation, the sol-gel method, or diffusion of Ag into silicon oxide by ion exchange, which require ions such as sodium¹⁹. However, here bonding was achieved at a low temperature via the native silicon oxide layer (comprising only silicon and oxygen), which reveals that such conventional formation processes cannot be available. On the other hand, the thin silicon oxide layer on the Si-material is likely to permit the diffusion of Ag ions, even at low temperatures (below 500 °C)^{24,38}. Actually, Ag was observed near the interface between Si and native oxide as shown in Fig. 6(b). Further, it was reported that Ag ions could adhere to the surface of silicon oxide²¹. In the present study, during the reaction between Ag₂O and the reducing solvent, silver carboxylate (R-COOAg) was temporarily formed, and subsequently Ag is thought to have precipitated as clusters or NPs along with the formation of gas, such as carbon dioxide and hydrogen oxide^{39–41}. It should be noted that no oxygen was generated during the reaction, implying that the oxidation of Si-materials never occurs. This assumption supports our results that no growth of the silicon oxide layer was observed at 300 °C. It is thought that Ag ions first adhered to the silicon oxide and then, with increasing temperature, either diffused (in small quantities) or formed nanoparticles on the surface of the silicon oxide. AgNPs locally precipitated as the result of supersaturation of diffused Ag in the silicon oxide, which conversely indicates that Ag atoms or ions would be present inside the layer, particularly near the interface. Accordingly, the formation of the interfacial structure below the thermal decomposition temperature would be as follows: (I) the generation of Ag ions due to the reaction between Ag₂O and organic solvent, (II) adhesion of Ag ions onto native oxide, (III) diffusion of Ag ions or atoms into the native oxide with increasing temperature, and (IV) precipitation of AgNPs followed by sintering. On the other hand, considering Si has a greater affinity for oxygen than Ag, the reaction between Ag₂O and Si described above (Reaction (2)) could not be negligible also for the presence of Ag in the SiO₂, i.e., corresponding to the step (III). Since the oxidation reaction of Si by Ag₂O involves the production of Ag and SiO₂, Ag could be confined by the produced SiO₂ on the native oxide at atomic scale. Nonetheless, the confined Ag would obey the step (IV).

Considering the formation of the interfacial structure above the thermal decomposition temperature of Ag_2O , we observed many AgNPs formed in the thick silicon oxide layer. As described above, it is widely known that the thermal decomposition of Ag_2O can finally result in AgNPs^{3,28,37}. Here we try to elucidate the formation of the silicon oxide layer containing AgNPs above 300–500 °C. Since no melting behaviour of silicon oxide occurred, the interfacial structure could be derived from several source: (i) confinement of generated Ag during the growth of silicon oxide, and (ii) thermal diffusion of Ag into silicon oxide. Concerning (i), Ag is confined by silicon oxide that is additionally formed on the surface of the native oxide as the result of reaction (2) described above; these reactions might occur repetitively. Since thermal decomposition occurs with a peak at around 400 °C, Ag should be present with a varying concentration distribution in the silicon oxide layer, corresponding to the observed experimental results. There are many reports regarding the oxidation mechanism in Si-materials; the oxidation mechanism changes with the thickness of the silicon oxide layer^{42–44}. In the case of a thin silicon oxide layer (below 20–30 nm), Si atoms emitted from the substrate couple with oxygen near the surface of silicon oxide, which causes fast oxidation. In contrast, inward diffusion of oxygen becomes more dominant than silicon diffusion with the increase in the thickness, and the growth of silicon oxide occurs either inside the layer or at the interface of the Si-material/silicon oxide (Deal-Grove model)⁴². The model is generally applicable for the oxidation progress corresponding to a thickness >20–30 nm. Therefore, the growth of silicon oxide occurs not at the surface but either inside the layer or at the interface of the Si-material/silicon oxide. In the present study, the thickness of the interfacial layer was about 50 nm. Therefore, the above mechanism (i) would be possible as the initial mechanism for the formation of interfacial structure since the oxidation of Si by Ag_2O at the surface of silicon oxide can occur up to 20–30 nm.

Considering mechanism (ii), some studies have reported the diffusion of Ag in silicon oxide despite the difficulties mentioned above. For instance, it was shown that Ag ions dissolved in glass, prepared by the mixture of glass frit with Ag paste, diffuses out^{45–47}. Further, in the case of an ion implanted SiO_2 film, it was observed that AgNPs precipitated in the SiO_2 at a deeper level than the implanted range after annealing at 500 °C^{48,49}. Actually, AgNPs were found inside the SiO_2 at a distance of several tens of nanometres from the SiO_2/Ag interface for the SiO_2 joint (Supplementary Fig. S5). These results implied the possibility of thermal diffusion of Ag atoms or ions below 500 °C. Assuming the thermal diffusion of Ag, we can explain the observed size- and concentration-distribution of the AgNPs in the silicon oxide layer. The Ag and oxygen concentrations would be distributed according to the thermal decomposition rate of Ag_2O dependent on the temperature, with a peak at about 400 °C. After the precipitation of AgNPs via the same precipitation mechanism below the thermal decomposition temperature, the size of AgNPs was in proportion to the concentrations, i.e., to the nearest-neighbour distances^{50,51}.

As above, the formation of the interfacial structure could be attributed to both mechanisms. Specifically, Ag would be initially present in silicon oxide owing both to the thermal diffusion of Ag and the confinement by silicon oxide through the oxidation of Si by Ag_2O . Subsequently, Ag would be present over the entire grown silicon oxide layer owing to the diffusion of Ag.

Such a formation process of the silicon oxide layer containing AgNPs is similar to that below the thermal decomposition temperature, where the presence of AgNPs is evidence of the existence of many Ag ions or atoms in the silicon oxide layer during bonding. Therefore, Ag atoms or ions inside the silicon oxide, particularly near the interface, should be available effectively for sufficient bonding between the silicon oxide and Ag in both cases.

It was indicated that the *in situ* formation of a silicon oxide layer containing Ag atoms contributes to the direct bonding of Ag and Si-materials in both temperature ranges. Herein, molecular dynamics simulations were used to elucidate the adhesion behaviour between Ag and SiO_2 . In order to verify the hypothesized mechanism, three kinds of amorphous SiO_2 substrate were analysed, SiO_2 substrates with Ag atoms embedded at d distance from the interface simulating the SiO_2 containing atomic Ag in correspondence with Fig. 4; d values were r , $2r$, and $3r$ where r is the Ag atomic radius. Figure 7 describe the adhesion of a AgNP onto the SiO_2 with Ag atoms embedded at (a) $d = r$ and (b) $d = 3r$. It was confirmed that a AgNP is not wet on the SiO_2 with Ag atoms embedded at $d = 3r$ at 500 °C, which reveals that there is no strong attractive force between Ag and SiO_2 atoms. In contrast, we found that AgNP can adhere to the SiO_2 with Ag atoms embedded at $d = r$ and $2r$ and increase the wetting angle. In addition, the layer should also contribute to the adhesion, even at 300 °C. It was reported that precipitated Ag in the SiO_2 layer remains in a metallic state⁵², indicating that Ag is present along the Ag/ SiO_2 interface and able to maintain the metallic bonding state. Therefore, it was revealed that the presence of Ag near SiO_2 surface played a significant role in establishing the bonding between Ag and Si-materials in either temperature range. Furthermore, it is also suggested that the interlayer between Ag and Si-materials can be designed by the control of the oxidation of Si-materials using the thermal decomposition process of Ag_2O paste.

Consequently, we found that the bonding between Ag and Si-materials was realized via *in-situ* formation of a silicon oxide layer containing AgNPs resulting from the different decomposition reactions of Ag_2O : (i) redox reaction between Ag_2O and the organic solvent, producing Ag ions and AgNPs, and (ii) thermal decomposition of Ag_2O producing Ag ions, AgNPs, and also oxygen, inducing oxidation of the Si-materials at low temperature. The dominant decomposition reaction can be controlled by the initial Ag_2O paste design or control of the thermal process. Thus, this method is expected to enable the implementation of various bonds with Si-materials; not only low-temperature direct bonding, but also direct fabrication of MOS structures and the production of conductive films by controlling the Ag concentration and SiO_2 layer thickness. Furthermore, in addition to bonding processes, the decomposition reaction of Ag_2O could be widely applied in various fields, such as the fabrication of conductive paths in various materials²⁸, and development of the screen-printing process for solar cells^{45,46}.

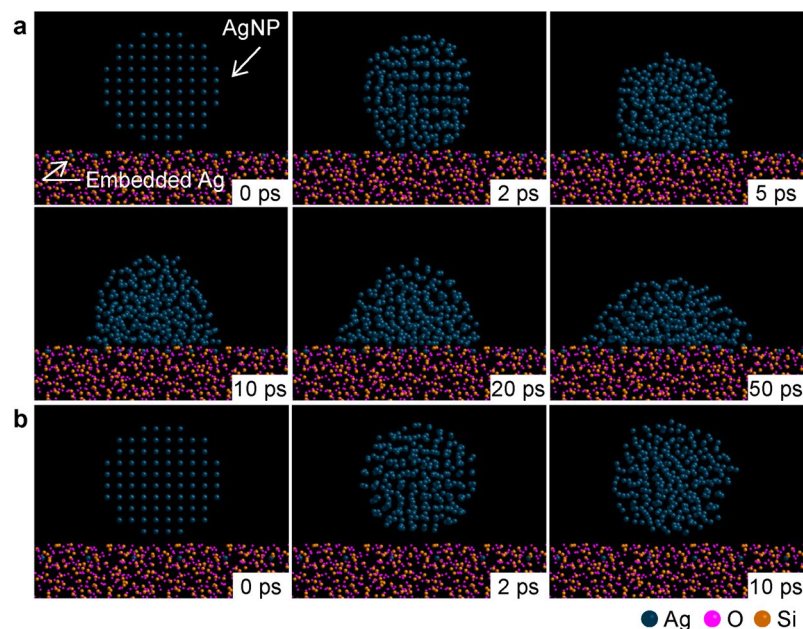


Figure 7. Adhesion behaviour of AgNP onto SiO₂ dependent on the interfacial structure of SiO₂, determined via molecular modelling. **(a)** Adhesion process of AgNP onto the SiO₂ surface with an embedded atomic Ag layer at $d = 1r$ from the surface. AgNP can adhere to SiO₂ with increasing wetting angle owing to the presence of embedded Ag atoms. **(b)** Desorption process of AgNP from SiO₂ with an embedded Ag layer at $d = 3r$ from the surface, showing no attractive force between the AgNP and SiO₂ layer. These simulations were performed at 500 °C.

Methods

Paste Preparation and characterization. Commercial silver oxide (I) (Ag₂O) particle diameters of 2–3 μm (Kojundo Chemical Laboratory Co. Ltd.) were used as the bonding material. The particles were milled for 10 min using an agate mortar and mixed with diethylene glycol (C₄H₁₀O₃) as the organic agent at a concentration of 180 μl/g. The mixture was processed to form a Ag₂O paste for bonding using a planetary centrifugal mixer (Thinky AR-100). The thermal characteristics of the Ag₂O paste were measured by performing differential thermal analysis (DTA) and thermogravimetric analysis (TGA) (Rigaku TG8120) at a heating rate of 60 °C/min in air.

Bonding Processing. Si wafers with a (100) orientation (Komatsu Silicon America, Inc.), polycrystalline silicon carbide (SiC) prepared by sintering (Kyocera Co., Ltd.), and amorphous silicon dioxide (SiO₂) (Kojundo Chemical Laboratory Co., Ltd) were used as the Si-material substrates for bonding. The dimensions were 10 mm × 10 mm × 0.6 mm or Si, 10 mm × 10 mm × 1 mm for SiC, and 10 mm in diameter × 5 mm for SiO₂. Gold (Au) discs with 5 mm diameter and 2 mm thickness were used as the metal substrate, which was fabricated by nickel/gold plating with a thickness of 3 μm and 1 μm, respectively, on a copper disc. Ag₂O paste was applied to the surface of the Si-material substrates with a thickness of 50 μm and then preheated at 100 °C. The Au substrate was placed on the Ag₂O paste layer after preheating. The samples were heated to the bonding temperature of 300–500 °C at a rate of 60 °C/min in an infrared heating furnace under air condition and held for 5 min with a pressure of 5 MPa. The samples were cooled by forced air after bonding.

Experimental Characterizations. In order to evaluate the influence of bonding temperature on the bond quality, the shear strengths of Au/Si-material joints bonded at 300–500 °C with a pressure of 5 MPa were measured with a strain rate of 30 mm/min. The shear strength was evaluated as the average value of three joints, and the error bars were determined as the standard deviation values. The joint microstructures were observed using a stereomicroscope (Olympus SZX7). The cross-sectioned joints were prepared by using a cross-section polisher (JEOL SM-09010) and observed using a scanning electron microscope (SEM; Hitachi S-3000H). The interfacial microstructure between the sintered Ag layer and the Si-materials was investigated using transmission electron microscopy (TEM; JEOL JEM-2100F) combined with energy dispersive X-ray spectroscopy (EDS). Thin foil samples for TEM observations were prepared using a focused ion beam method (FIB; JEOL JIB-4500).

Molecular Dynamics simulations. Calculations of the adhesion behaviour of AgNP onto SiO₂ were performed using the commercial molecular dynamics software SCIGRESS ME 2.0 (Fujitsu). For the potential functions, Generalized Embedded Atom potential (Ag–Ag), Morse potential (Si–O), and ME3Organic potential (Ag–N, Ag–O and Ag–Si), which are included in the MD software package, were used. The simulated temperature and pressure were set to 500 °C and 1 atm, respectively. The SiO₂ substrate was designed as amorphous and Ag atoms were embedded at $d = r, 2r$ and $3r$, where r is the atomic radius of Ag, from the surface of the substrate. The diameter of the AgNP on SiO₂ was 2 nm.

Data availability. The datasets generated and analysed during the current study are available from the corresponding author upon reasonable request.

References

- Kisiel, R. & Szczepaski, Z. Die-attachment solutions for SiC power devices. *Microelectron. Reliab.* **49**, 627–629 (2009).
- Zhang, H., Nagao, S., Suganuma, K., Albrecht, H.-J. & Wilke, K. Thermostable Ag die-attach structure for high-temperature power devices. *J. Mater. Sci. Mater. Electron* **27**, 1337–1344 (2016).
- Lin, S. *et al.* Nano-volcanic Eruption of Silver. *Sci. Rep.* **6**, 34769, <https://doi.org/10.1038/srep34769> (2016).
- Li, J., Johnson, C. M., Buttay, C., Sabbah, W. & Azzopardi, S. Bonding strength of multiple SiC die attachment prepared by sintering of Ag nanoparticles. *J. Mater. Proc. Technol.* **215**, 299–308 (2015).
- Bai, J. G., Yin, J., Zhang, Z., Lu, G. Q. & Wyk, J. D. High-temperature operation of SiC power devices by low-temperature sintered silver die-attachment. *IEEE Trans. Adv. Packag.* **30**, 506–510 (2007).
- Morita, T., Yasuda, Y., Ide, E., Akada, Y. & Hirose, A. Bonding Technique Using Micro-Scaled Silver-Oxide Particles for *In-Situ* Formation of Silver Nanoparticles. *Mater. Trans.* **49**, 2875–2880 (2008).
- Hirose, A. *et al.* A novel metal-to-metal bonding process through *in-situ* formation of Ag nanoparticles using Ag₂O microparticles. *J. Phys. Conf. Ser.* **165**, 012074 (2009).
- Allen, G. L., Bayles, R. A., Gile, W. W. & Jesser, W. A. Small particle melting of pure metals. *Thin Sol. Films* **144**, 297–308 (1986).
- Goldstein, A. N., Echer, C. M. & Alivisatos, A. P. Melting in Semiconductor Nanocrystals. *Science* **256**, 1425–1427 (1992).
- Lai, S. L., Guo, J. Y., Petrova, V., Ramanath, G. & Allen, L. H. Size-Dependent Melting Properties of Small Tin Particles: Nanocalorimetric Measurements. *Phys. Rev. Lett.* **77**, 99–102 (1996).
- Klabunde, K. J. *et al.* Nanocrystals as Stoichiometric Reagents with Unique Surface Chemistry. *J. Phys. Chem.* **100**, 12142–12153 (1996).
- Morita, T., Yasuda, Y., Ide, E. & Hirose, A. Direct Bonding to Aluminum with Silver-Oxide Microparticles. *Mater. Trans.* **50**, 226–228 (2009).
- Takata, S., Ogura, T., Ide, E., Morita, T. & Hirose, A. Effects of Solvents in the Polyethylene Glycol Series on the Bonding of Copper Joints Using Ag₂O Paste. *J. Electron. Mater.* **42**, 507–515 (2013).
- Ogura, T., Takata, S., Takahashi, M. & Hirose, A. Effects of Reducing Solvent on Copper, Nickel, and Aluminum Joining Using Silver Nanoparticles Derived from a Silver Oxide Paste. *Mater. Trans.* **56**, 1030–1036 (2015).
- Asama, K. *et al.* Low-temperature metal-to-alumina direct bonding process utilizing redox reaction between silver oxide and organic agent. *Mater. Sci. Eng. A* **702**, 398–405 (2017).
- Sakamoto, S., Nagao, S. & Suganuma, K. Thermal fatigue of Ag flake sintering die-attachment for Si/SiC power devices. *J. Mater. Sci.: Mater. Electron.* **24**, 2593–2601 (2013).
- Smith, P. H. & Gurev, H. Silicon dioxide as a high temperature stabilizer for silver films. *Thin Sol. Films* **45**, 159–168 (1977).
- Doremus, R. H. Exchange and diffusion of ions in glass. *J. Phys. Chem.* **68**, 2212–2218 (1964).
- Simo, A. *et al.* Formation Mechanism of Silver Nanoparticles Stabilized in Glassy Matrices. *J. Am. Chem. Soc.* **134**, 18824–18833 (2012).
- Tzounis, L. *et al.* Controlled growth of Ag nanoparticles decorated onto the surface of SiO₂ spheres: a nanohybrid system with combined SERS and catalytic properties. *RSC Adv.* **4**, 17846–17855 (2014).
- Cai, Y. *et al.* Room-temperature synthesis of silica supported silver nanoparticles in basic ethanol solution and their antibacterial activity. *RSC Adv.* **6**, 18407–18412 (2016).
- Tang, S., Tang, Y., Gao, F., Liu, Z. & Meng, X. Ultrasonic electrodeposition of silver nanoparticles on dielectric silica spheres. *Nanotechnology* **18**, 295607 (2007).
- Phatangare, A. B. *et al.* Surface chemical bonds, surface-enhanced Raman scattering, and dielectric constant of SiO₂ nanospheres *in-situ* decorated with Ag-nanoparticles by electron-irradiation. *J. Appl. Phys.* **120**, 234901 (2016).
- McBrayer, J. D., Swanson, R. M. & Sigmon, T. W. Diffusion of Metals in Silicon Dioxide. *J. Electrochem. Soc.* **133**, 1242–1246 (1986).
- Cattaruzza, E., Gonella, F., Ali, S., Sada, C. & Quaranta, A. Silver and gold doping of SiO₂ glass by solid-state field-assisted diffusion. *J. Non-Cryst. Solids* **355**, 1136–1139 (2009).
- Waterhouse, G. I. N., Bowmaker, G. A. & Metson, J. B. The thermal decomposition of silver (I, III) oxide: A combined XRD, FT-IR and Raman spectroscopic study. *Phys. Chem. Chem. Phys.* **3**, 3838–3845 (2001).
- Chiu, Y. *et al.* Fabrication and nonlinear optical properties of nanoparticle silver oxide films. *J. Appl. Phys.* **94**, 1996–2001 (2003).
- Matsuhisa, N. *et al.* Printable elastic conductors by *in situ* formation of silver nanoparticles from silver flakes. *Nat. Mater.* **16**, 834–840 (2017).
- Shi, Y. *et al.* Investigation of rare earth-doped BiAg high-temperature solders. *J. Mater. Sci. Mater. Electron.* **21**, 875–881 (2010).
- Ide, E., Hirose, A. & Kobayashi, K. F. Influence of bonding condition on bonding process using Ag metallo-organic nanoparticles for high temperature lead-free packaging. *Mater. Trans.* **47**, 211–217 (2006).
- Stookey, S. D. Coloration of glass by gold, silver, and copper. *J. Am. Ceram. Soc.* **32**, 246–249 (1949).
- Hamzaoui, H. E., Capoen, B., Razdobreev, I. & Bouzaoui, M. *In situ* growth of luminescent silver nanoclusters inside bulk sol-gel silica glasses. *Mater. Res. Exp.* **4**, 076201 (2017).
- L'vov, B. V. Kinetics and mechanism of thermal decomposition of silver oxide. *Thermochim. Acta* **333**, 13–19 (1999).
- Fields, J. D. *et al.* The formation mechanism for printed silver-contacts for silicon solar cells. *Nat. Commun.* **7**, 11143, <https://doi.org/10.1038/ncomms11143> (2016).
- Pilling, N. & Bedworth, R. The Oxidation of Metals at High Temperatures. *J. Inst. Metals* **29**, 529–591 (1923).
- Leroy, B. Stresses and silicon interstitials during the oxidation of a silicon substrate. *Philos. Mag. B* **55**, 159–199 (1986).
- Yasuda, Y., Ide, E. & Morita, T. Low-Temperature Bonding Using Silver Nanoparticles Stabilized by Short-Chain Alkylamines. *Jpn. J. Appl. Phys.* **48**, 125004 (2009).
- Horváth, B., Kawakita, J. & Chikyov, T. Diffusion barrier and adhesion properties of SiO_xN_y and SiO_x layers between Ag/polypyrrole composites and Si substrates. *ACS Appl. Mater. Interfaces* **6**, 9201–9206 (2014).
- Luo, C., Zhang, Y., Zeng, Y. & Wang, Y. The role of poly(ethylene glycol) in the formation of silver nanoparticles. *J. Colloid Interface Sci.* **288**, 444–448 (2005).
- Fields, E. K. & Meyerson, S. Thermal and Photochemical Decomposition of Silver Carboxylates. *J. Org. Chem.* **41**, 916–920 (1976).
- Zhang, R., Lin, W., Moon, K. & Wong, C. P. Fast Preparation of Printable Highly Conductive Polymer Nanocomposites by Thermal Decomposition of Silver Carboxylate and Sintering of Silver Nanoparticles. *ACS Appl. Mater. Interfaces* **2**, 2637–2645 (2010).
- Deal, B. E. & Grove, A. S. General Relationship for the Thermal oxidation of Silicon. *J. Appl. Phys.* **36**, 3770–3778 (1965).
- Ibano, K., Itoh, K. M. & Uematsu, M. Generation of excess Si species at Si/SiO₂ interface and their diffusion into SiO₂ during Si thermal oxidation. *J. Appl. Phys.* **103**, 026101 (2008).
- Song, Y., Dhar, S., Feldman, L. C., Chung, G. & Williams, J. R. Modified Deal Grove model for the thermal oxidation of silicon carbide. *J. Appl. Phys.* **95**, 4953–4957 (2004).
- Lin, C.-H., Tsai, S.-Y., Hsu, S.-P. & Hsieh, M.-H. Investigation of Ag-bulk/glassy-phase/Si heterostructures of printed Ag contacts on crystalline Si solar cells. *Sol. Energy Mater. Sol. Cells* **92**, 1011–1015 (2008).

46. Cho, S.-B., Kim, H.-S. & Huh, J.-Y. Mechanism underlying the beneficial effect of forming gas annealing on screen-printed Ag contacts of crystalline Si solar cells. *Acta Mater.* **70**, 1–7 (2014).
47. Qin, J., Zhang, W., Bai, S. & Liu, Z. Study on the sintering and contact formation process of silver front side metallization pastes for crystalline silicon solar cells. *Appl. Surf. Sci.* **376**, 52–61 (2016).
48. Tsuji, H. *et al.* Delta layer formation of silver nanoparticles in thin silicon dioxide film by negative ion implantation. *Surf. Coat. Technol.* **196**, 39–43 (2005).
49. Arai, N. *et al.* Nanocrystal Formation of Metals in Thermally Grown Thin Silicon Dioxide Layer by Ion implantation and Thermal Diffusion of Implanted Atoms in Heat Treatment. *J. Phys. Conf. Ser.* **61**, 41–45 (2007).
50. Kumar, P. *et al.* Plasmonic resonance of Ag nanoclusters diffused in soda-lime glasses. *Phys. Chem. Chem. Phys.* **17**, 8596–8603 (2015).
51. Stepanov, A. L. Synthesis of silver nanoparticles in dielectric matrix by ion implantation: A review. *Rev. Adv. Mater. Sci.* **26**, 1–29 (2010).
52. Babapour, A., Akhavan, O., Azimirad, R. & Moshfegh, A. Z. Physical characteristics of heat-treated nano-silvers dispersed in sol-gel silica matrix. *Nanotechnology* **17**, 763–771 (2006).

Acknowledgements

The authors would like to thank Professor M. Takahashi and K. Ito of Osaka University for his significant help with the TEM observations. This study was performed in part under the Cooperative Research Program of Institute for Joining and Welding Research Institute, Osaka University. This work was supported in part by JSPS KAKENHI Grant Number JP26289248 and JP18K14028.

Author Contributions

T.M., T.S. and A.H. conceived the study and drafted the manuscript. T.M., K.I. and K.M. performed the experiments. T.M., K.I. and K.M. analysed the data. The manuscript was written by T.M. All authors contributed to the data analysis and interpretation of the results through discussion.

Additional Information

Supplementary information accompanies this paper at <https://doi.org/10.1038/s41598-018-28788-x>.

Competing Interests: The authors declare no competing interests.

Publisher's note: Springer Nature remains neutral with regard to jurisdictional claims in published maps and institutional affiliations.



Open Access This article is licensed under a Creative Commons Attribution 4.0 International License, which permits use, sharing, adaptation, distribution and reproduction in any medium or format, as long as you give appropriate credit to the original author(s) and the source, provide a link to the Creative Commons license, and indicate if changes were made. The images or other third party material in this article are included in the article's Creative Commons license, unless indicated otherwise in a credit line to the material. If material is not included in the article's Creative Commons license and your intended use is not permitted by statutory regulation or exceeds the permitted use, you will need to obtain permission directly from the copyright holder. To view a copy of this license, visit <http://creativecommons.org/licenses/by/4.0/>.

© The Author(s) 2018